Frontiers in Earth Science

TYPE Review
PUBLISHED 17 March 2025
DOI 10.3389/feart.2025.1560988

Geochemical characteristics and tectonic implications of igneous rocks from the Santos Basin and adjacent areas

Jinglin Su[1,2†], Jing Sun[1,2*†] and Liu Yang[3]

[1]State Key laboratory of Petroleum Resources and Engineering, Beijing, China, [2]College of Geosciences, China University of Petroleum, Beijing, China, [3]PetroChina Hangzhou Research Institute of Geology, Hangzhou, China

OPEN ACCESS

EDITED BY
Wei-Qiang Ji,
Chinese Academy of Sciences (CAS), China

REVIEWED BY
Guo Chang Wang,
Yunnan University, China
Hao Yang,
Jilin University, China

*CORRESPONDENCE
Jing Sun,
sunjingvv@163.com

†These authors have contributed equally to this work

RECEIVED 15 January 2025
ACCEPTED 20 February 2025
PUBLISHED 17 March 2025

CITATION
Su J, Sun J and Yang L (2025) Geochemical characteristics and tectonic implications of igneous rocks from the Santos Basin and adjacent areas.
Front. Earth Sci. 13:1560988.
doi: 10.3389/feart.2025.1560988

The increasing presence of igneous rocks in hydrocarbon-bearing basins are drawing more attention. While the roles they play during the hydrocarbon generation and reservoir formation remain poorly understood, yet a detailed inspection of their geochemical features within the corresponding tectonic context is lacking. This study compiles comprehensive geochemical data, including major and trace elements, as well as the isotopic composition of igneous rocks spanning from 147 to 40 Ma at the Santos Basin and adjacent area. Based on their geochemical signatures and tectonic settings, the igneous rocks are classified and analyzed. During 147–40 Ma, the studied location had a complex tectonic background which demonstrated a transition from the mantle plume to continental rift, then to mantle plume, corresponding to the discovered geochemical characteristics. This progression corresponds to the breakup of the West Gondwana and the opening of the South Atlantic Ocean. The findings highlight the potential positive role of igneous rocks in hydrocarbon systems, revealing their potential favorable roles. These results provide a robust foundation for future exploration and research in analogous basins.

KEYWORDS

Santos basin, igneous rock, gondwana, south atlantic opening, mantle plume

1 Introduction

The exploration of petroleum resources traditionally focused on sedimentary strata; however, recent research underscores the significant role of igneous rocks in hydrocarbon systems. Studies reveal that volcanic activities can influence hydrocarbon generation and reservoir formation through processes including modifying depositional environments and catalyzing hydrocarbon generation and so on. Globally, igneous rocks' presences in hydrocarbon reservoirs are increasingly recognized for their potential, with major discoveries in regions such as Bohai Bay Basin, Sichuan Basin, and Northern JiangSu Basin (Guo et al., 2022; Luo et al., 2019; Mu and Ji, 2019; Wang et al., 2015; Jiang et al., 2011; Jin and Zhai, 2003). While the role igneous rocks played was historically overlooked, their importance has been validated by discoveries such as those in the Daqing Oilfield and the Dongying Sag, where volcanic rocks provide ideal reservoir spaces, pivotal age information and catalysts in hydrocarbon generation (Chen et al., 2018; Song, 2009; Jin et al., 2006; Zhai et al., 2004; Jin and Zhai, 2003; Wan et al., 2003). The presence of igneous rocks in petroleum systems generally indicates destruction, making them unfavorable. But these cases challenge the traditional perspective of avoiding igneous rocks in petroleum exploration. On the contrary, these igneous rocks offer critical insights into the interplay between magmatism and basin tectonics, even the hydrocarbon systems.

The Santos Basin, located on the passive continental margin of Brazil, presents an ideal case study for exploring the role of igneous rocks in the rift basin along the continental margin. As a petroleum-producing basin, it features a significant presence of igneous rocks. Additionally, the multiple episodes of igneous rocks interbed with the sedimentary layers make it unique for understanding the relationship between oil generation and rift basin development (Mohriak et al., 2012). In previous research, geophysical studies have classified the basin's tectonic stages and coeval magmatic movements, while geochronological analyses of igneous rocks have established their different periods. However, a detailed investigation into the geochemical features and their tectonic implications remains insufficient.

In this study, we collected the geochemical and geochronological data of igneous rocks from the Santos Basin and adjacent areas at various ages. We compiled the data and classified the igneous rocks into different periods based on their age information and correlated tectonic backgrounds. Through the geochemical analysis on each episode of igneous rock, their unique features and tectonic implications are revealed. An overlook of the tectonic history in the studied areas is also proposed.

2 Geological background

The Santos Basin is a large sedimentary basin located on southeastern Brazil's coast, recognized as part of the South Atlantic passive margin. The Santos basin is bounded by Cabo Frio High to the north and Florianópolis to the south, covering an area of approximately 350,000 km^2. So far, the Santos Basin, has become one of the many major locations for global oil and gas exploration, with more than 15 blocks that each have petroleum reserves over 1.0×10^9 bbl, shedding insight into ultra-deep water and pre-salt exploration technologies. Next to the Santos Basin, there also are localities that develop large amounts of igneous rocks, including Campos Basin and Paraná Basin (Figure 1). The Campos Basin, situated north of the Santos Basin, is bounded by the Vitória High to the north and lies adjacent to it in the southern direction, and has coverage of 100,000 km^2 with yet-to-discovered recoverable oil and gas resources of about 3.3×10^9 bbl. The Paraná Basin, on the other hand, recognized as the largest in Brazil, stands as one of the most significant oil-bearing basins in South America. (Anjos et al., 2024; Yu et al., 2022; Zhang et al., 2020; Buckley et al., 2015; Moreira et al., 2007; Liu and Liu, 2006).

Formed as basins along the passive continental margin, the abundance of magma movements must be correlated to the process of West Gondwana breaking and the South Atlantic Opening. In the Neoproterozoic era, West Gondwana formed primarily through the collision between Brasiliano-Pan African orogeny (Feng et al., 2024; Suárez et al., 2021). In the Mesozoic era, the West Gondwana started breaking along with the opening of the South Atlantic Ocean (Eagles and Eisermann, 2020; Feng et al., 2024). Both the continental drift and seafloor spreading led to the further separation of the continental masses and shaped the ocean formation. As a result, multiple episodes of volcanic activities closely tied to the tectonic movements happened along the continental margin, just as recorded in these locations (Eagles, 2007; Torsvik et al., 2009; Gao, 2022).

Having outlined the tectonic and sedimentary history of the basin, it is crucial to investigate the stratigraphy of the Santos Basin, as it reflects the basin's evolutionary stages and sedimentary processes through lithological features, particularly the presence of igneous rocks. Developed on the pre-Cambrian crystalline basement, the Santos Basin has been classified into three distinct evolution phases based on tectonostratigraphic evidence: rift, post-rift, and drift, as proposed by Moreira et al. (2007). The rift sequences contain Camboriu, Picarras, and Itapema Formations, consisting of volcanic rocks (Camboriu), lake sediments (Picarras), coquinas and dark shales (Itapema). The post-rift sequences include Barra Velha and Ariri Formations, comprising microbialites, stromatolites (Barra Velha), and evaporites (Ariri). The drift sequences are composed of Florianópolis, Guarujá, Itanhaém Formations, mainly carbonate rocks and sandstones. In general, the geological sequences in the area feature igneous rocks within the rift sequences, along with interlayering of igneous and sedimentary strata, showing a complex interplay of different rock types.

3 Geochronology

The Santos Basin and adjacent areas contain multiple episodes of igneous rocks belonging to different magmatic durations, ranging from 147 Ma to 40 Ma. Rock types contain lamprophyre, basalt, diabase, andesite, kimberlite, syenite and phonolite. The dividing of these magmatic activities is still in debated.

Cheng et al. (2019) distinguished Santos Basin igneous rocks into three periods based on fault activities. (1) Rift phase (125–120 Ma). Determined by the borehole samples from drilled igneous rocks, the rift phase was dated to 125–120 Ma through $^{40}Ar/^{39}Ar$ isotopic analysis, indicating severe magmatic activities in the Early Cretaceous era. (2) Sag phase (~110 Ma). Judged by sagging movements and Rift-Sag transition, less active than the Rift phase, the Sag phase was dated to ~110 Ma through volcanic rock $^{40}Ar/^{39}Ar$ isotopic analysis. (3) Drift phase (90–70 Ma). With fault intensity close to the Sag phase, the Drift phase marked another episode of magmatic movement, dated back to 90–70 Ma by volcanic rock $^{40}Ar/^{39}Ar$ isotopic analysis.

Some studies introduced refined classifications by integrating geochronological, geochemical, and geophysical data. For example, Wang et al. (2018) concluded the basin-wide magmatic activities into four periods, followed as (1) Valanginian-Hauterivian (139–129 Ma), (2) Aptian (125–113 Ma), (3) Santonian-Campanian (86–72 Ma), (4) Eocene (56–33.9 Ma). In this research, instead of using exact age information, the igneous rocks were classified into different episodes based on chronostratigraphic periods, combining evidence from geophysical studies, including seismic profiles, distribution of fracture zones as well as gravity anomalies. Similarly, Gordon et al. (2023) adjusted the magmatic framework by

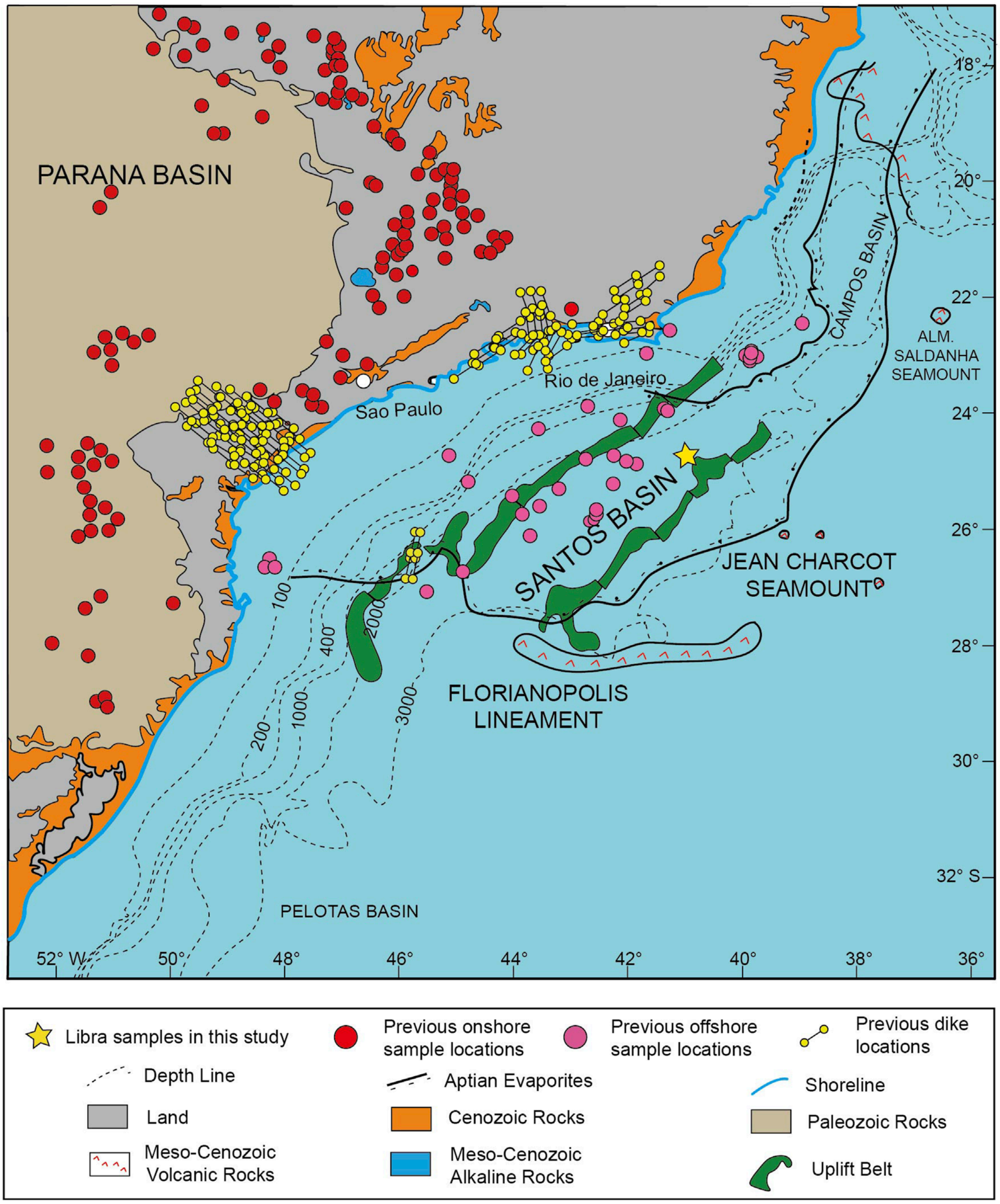

FIGURE 1
The geological map of the study area and locations of data points in Southeast Brazil. Modified from He et al. (2025).

integrating isotopic age data (including $^{40}K/^{40}Ar$, $^{40}Ar/^{39}Ar$, U-Pb age information) with tectonic contexts, identifying phases such as the Pre-Rift phase (135–132 Ma), the Rift phase (130–123 Ma), the Post-Rift phase (123–112 Ma), the Drift phase (112–23.3 Ma).

Recently, Liu et al. (2023) added emplacement-based distinctions and further divided the igneous rocks into more periods: (1) Valanginian-Hauterivian extrusive rock, (2) Barremian-Aptian extrusive rock, (3) Aptian extrusive rock, (4) Campanian intrusive rock, (5) Eocene extrusive rock, (6) Eocene intrusive rock. The exact geochronological information based on raw $^{40}Ar/^{39}Ar$ data in combination with a comprehensive interpretation of geochemical features are provided (He et al., 2025). The intrusive rocks have ages of 126–121 Ma based on whole rock and plagioclase $^{40}Ar/^{39}Ar$ isotope analysis, and the extrusive rocks are generally older than extrusive ones but belong to the same episode.

In summary, existing classifications of magmatic activity in the Santos Basin vary widely, reflecting differences in methodologies and focal points, including tectonic phases, chronostratigraphy,

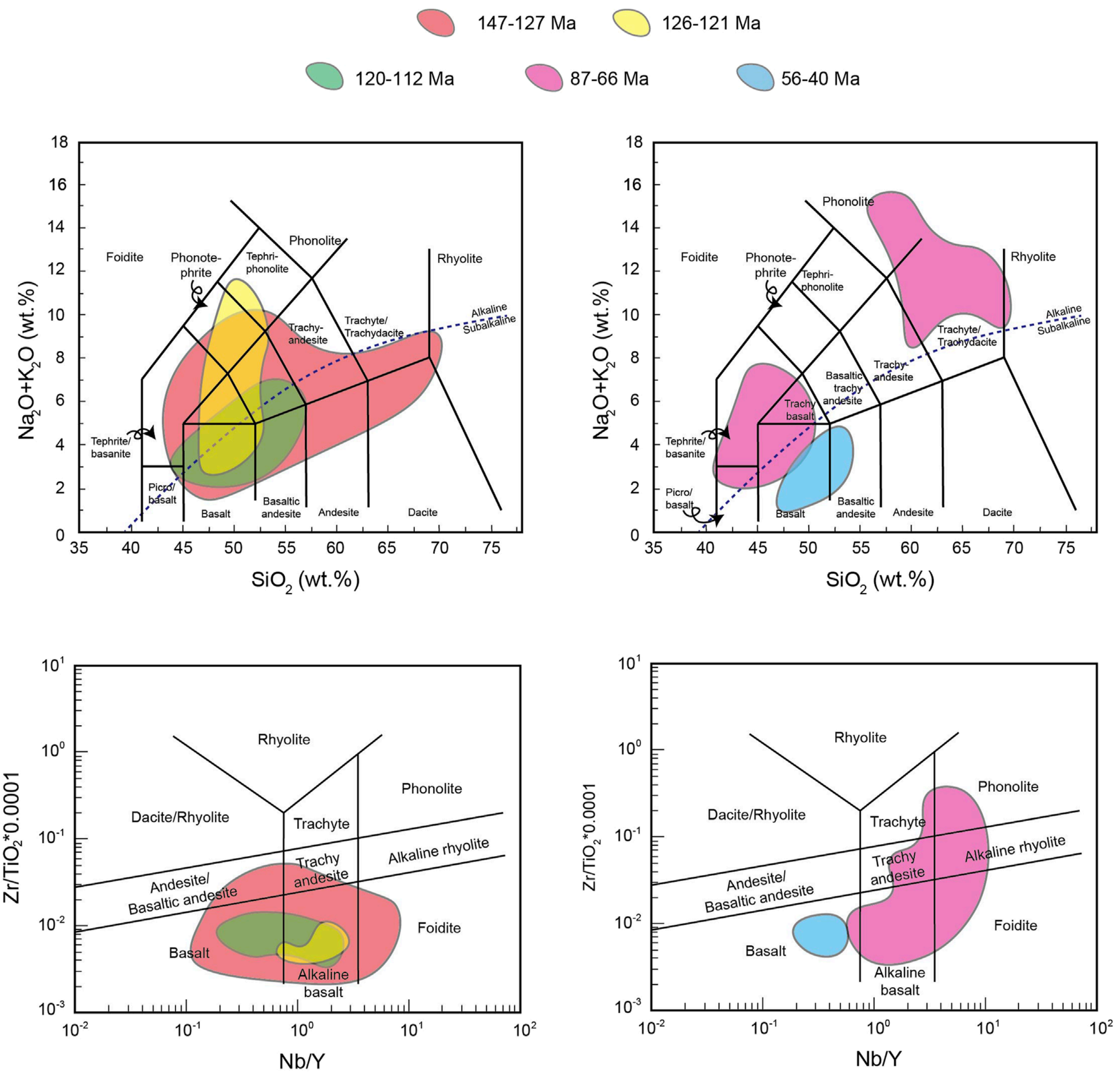

FIGURE 2
TAS discrimination diagram and Nb/Y vs. Zr/TiO_2 diagram of igneous rocks from 147 Ma to 40 Ma. Classification after Bas et al. (1986) and Winchester and Floyd., (1977) respectively. All data are provided in Supplementary Material.

isotopic dating, and emplacement locations. While these studies provide valuable insights, discrepancies remain in defining precise time spans and linking magmatic episodes to geochemical and tectonic contexts.

Building on these foundations and based on rock geochemistry and petrological principles, variations in igneous episodes are usually expected to represent comprehensive changes in magma genesis and geochemical characteristics. Therefore, after the analysis of geochemical characteristics, including major, trace elements and isotopic compositions, the magma sources and geochronological information are compared with the regional tectonic background. Based on the above process, the tectonic movements corresponding to each period reveal a transition from mantle plume activity, continental rift, and mantle plume. Such a progression reflects an igneous rock sequence that was first initiated by the mantle plume dynamic, then the expansion of continental rift, and lastly, the reactivation of another mantle plume process. Thus, we suggest that the igneous rocks from Santos basins and adjacent areas should be divided into five episodes: (1) 147–127 Ma; (2) 126–121 Ma; (3) 120–112 Ma; (4) 87–66 Ma; and (5) 55–40 Ma. Furthermore, the geochemical characteristics, encompassing major, trace, and isotopic compositions, correspond closely with the tectonic context of each episode. This refined temporal classification not only offers a more precise adjustment, but also incorporates the geological evolutionary history of the region within its tectonic context, thereby providing a scientific basis for a deeper understanding of the formation of the igneous rocks and their tectonic control in southeastern Brazil.

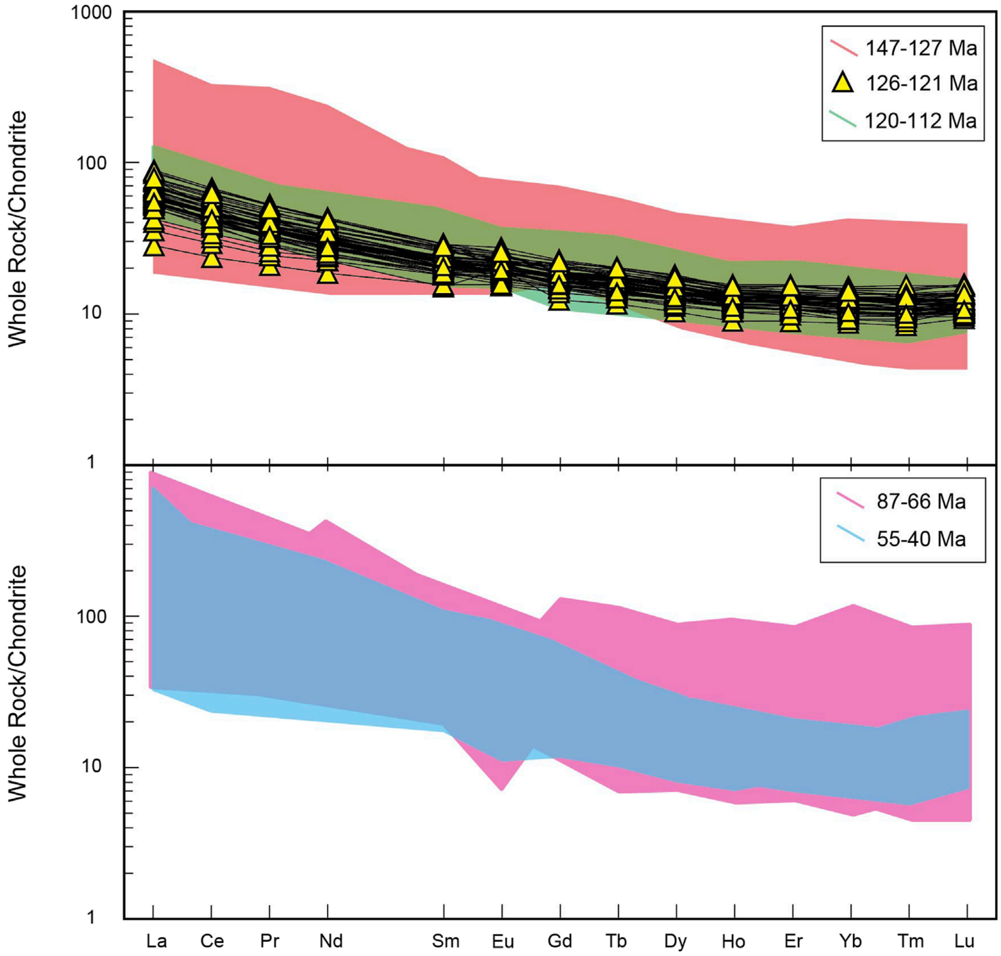

FIGURE 3
Chondrite normalized rare earth elements spidergram of igneous rocks from 147 Ma to 40 Ma. Chondrite data are from Sun and McDonough (1989). All data are provided in Supplementary Material.

4 Geochemical characteristics of multiple episodes of igneous rocks

4.1 147–127 ma igneous rocks' characteristics

During this period, the main lithotypes include basalt, diabase, basaltic andesite and dacite. The dominant lithology comprises basic rocks exhibiting pronounced alkaline characteristics, with trace element and isotopic signatures suggesting a potential association with mantle plume activity. Both Total Alkaline vs Silica discrimination (TAS) and Zr/Ti vs Nb/Y diagram (Figure 2) indicate that the majority of rocks at this period plot into the basalt and basaltic fields with alkaline series and subalkaline series both present, and only a small portion is scattered in intermediate and acidic rock fields. The 147–127 Ma igneous rocks exhibit strong enrichment in Light Rare Earth Elements (LREEs) and depletion in Heavy Rare Earth Elements (HREEs) (Figure 3). The Large-ion Lithophile Elements (LILE) also enriched over the High Field-Strength Elements (HFSE), with enrichment in Ba, U, Ta, and depletion in Th (Figure 4). The initial $^{87}Sr/^{86}Sr$ values show a wide range, varying from 0.703,596 to 0.717,578, with the majority showing enriched signature. Similarly, they also show enriched Nd isotopic compositions, with $^{143}Nd/^{144}Nd$ values ranging from 0.511,384 to 0.512,777, with negative $\varepsilon Nd_{(t)}$ values for majority samples (−0.7 to −21.21) (Figure 5).

4.2 126–121 ma igneous rocks' characteristics

Between 126 and 121 Ma, basalts, diabases and a small portion of dacites were emplaced in both Paraná and Santos Basin (Figure 2). Compared with igneous rocks from Santos Basin, the 126–121 Ma igneous rocks from Paraná Basin have higher SiO_2 content (48.70%–57.60% vs 36.92%–47.54%). Rocks emplaced in these two areas displayed enriched LREE and depleted HREE (Figure 3), and LILE enriched over HSFE (Figure 4). Meanwhile, they show decoupled Sr-Nd isotopes. The initial $^{87}Sr/^{86}Sr$ values have a rather wide range, from 0.704,609 to 0.709,684, whereas the initial $^{143}Nd/^{144}Nd$ values are 0.512,706–0.512,834, with $\varepsilon Nd_{(t)}$ +1.9 to +4.5 (Figure 5; He et al., 2025).

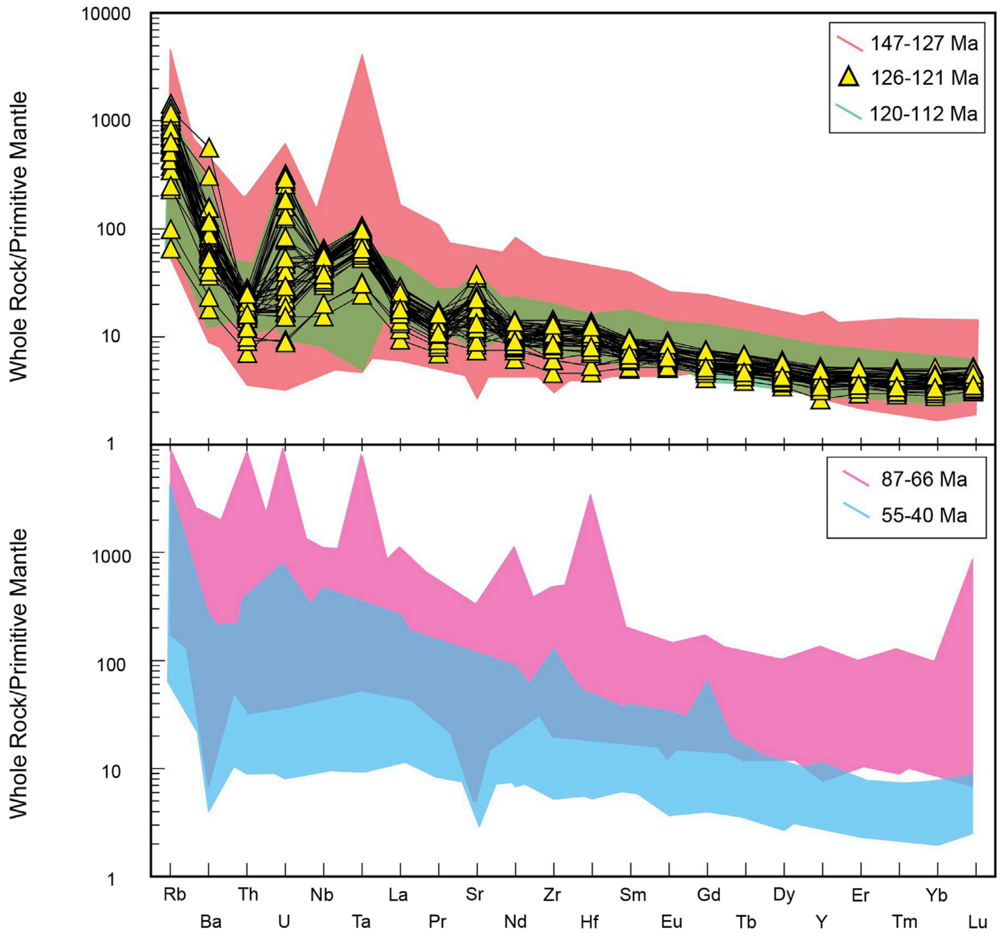

FIGURE 4
Primitive mantle normalized trace elements spidergram of igneous rocks from 147 Ma to 40 Ma. Primitive mantle data are from Sun and McDonough (1989). All data are provided in Supplementary Material.

4.3 120–112 ma volcanic rocks' characteristics

From 120 to 112 Ma, rocks are mainly subalkaline basaltic andesite and basalts (Figure 2). The MgO content varies from 2.10% to 8.05%, with one exception reaching 20.53%. This group of volcanic rocks has Na_2O + K_2O from 2.90% to 8.84%. The REE displays a pattern that LREE are more enriched than the HREE and have a narrower distribution range than earlier volcanic rocks (Figure 3). Strong enrichments exist in the Ba, U, and Ta, and depletion in Th (Figure 4). Both Sr and Nd isotopic compositions suggest an enriched characteristic, with $^{87}Sr/^{86}Sr$ values range from 0.705,804 to 0.706,804, and initial $^{143}Nd/^{144}Nd$ values ranging from 0.512,174 to 0.512,289 (Figure 5).

4.4 87–66 ma volcanic rocks' characteristics

During the interval of 87–66 Ma, rocks are mainly syenite, lamprophyre, tephrite, phonolite and foidite. The acidic rocks emerge as the predominant lithotype, with most samples classified as alkaline (Figure 2). Compared with the earlier groups, the 87–66 Ma volcanic rocks display higher LREE enrichment over HREE, showing a greater degree of inclination in the diagram (Figure 3). Also, a distribution pattern where a more obvious enriched LILE and depleted HFSE, with depletion in Ba and Sr can be observed (Figure 4). They show enriched characteristics in Sr and Nd isotopic compositions, with initial $^{87}Sr/^{86}Sr$ values ranging from 0.704,530 to 0.708,250, and $^{143}Nd/^{144}Nd$ system varying from 0.512,370 to 0.512,550 (Figure 5).

4.5 55–40 ma volcanic rocks' characteristics

Between 55 and 40 Ma, the igneous rocks are phonolite and tholeiitic dykes. They predominantly consist of basic compositions with subalkaline characteristics. The MgO contents are 0.01%–12.98%, and the Na_2O + K_2O contents are from 1.38% to 18.51%. The 55–40 Ma volcanic rocks share similar inclination

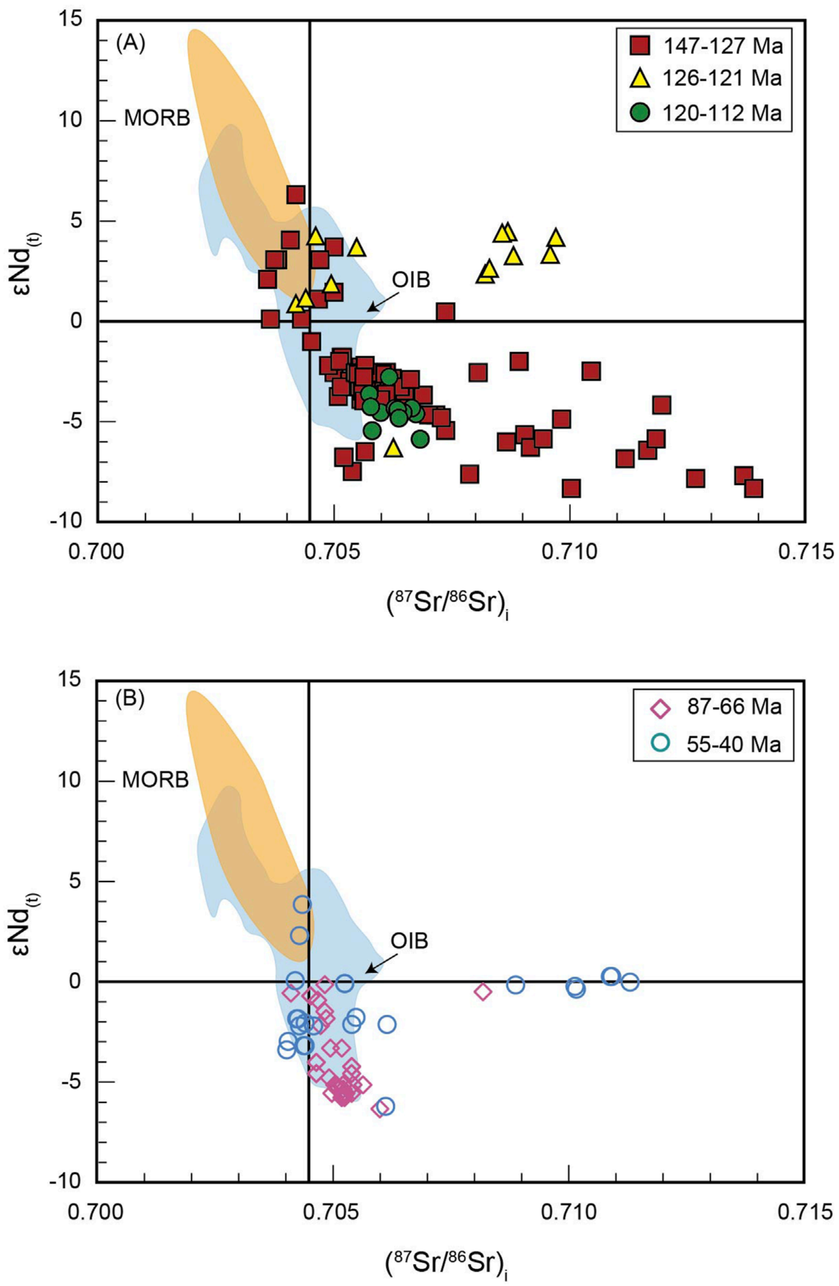

FIGURE 5
Whole-rock Sr-Nd isotopic composition of igneous rocks at 147-112 Ma **(A)** and 87-40 Ma **(B)**. All data are provided in Supplementary Material. MORB and OIB data are from the Pet DB database (https://search.earthchem.org/).

trends with early rocks, with LREE enriched and HREE depleted (Figure 3). They also display a similar pattern that LILE enriched over HSFE and depletions in Ba, Sr (Figure 4). The initial $^{87}Sr/^{86}Sr$ values are from 0.704,010 to 0.711,326, with most falling between 0.704,010 and 0.706,130. And the initial $^{143}Nd/^{144}Nd$ values range from 0.512,250 to 0.512,760, most of which show depleted signatures (Figure 5).

5 Discussion

5.1 Fractional crystallization and crustal contamination

Understanding the geochemical characteristics of igneous rocks is crucial for unraveling their formation processes and tectonic

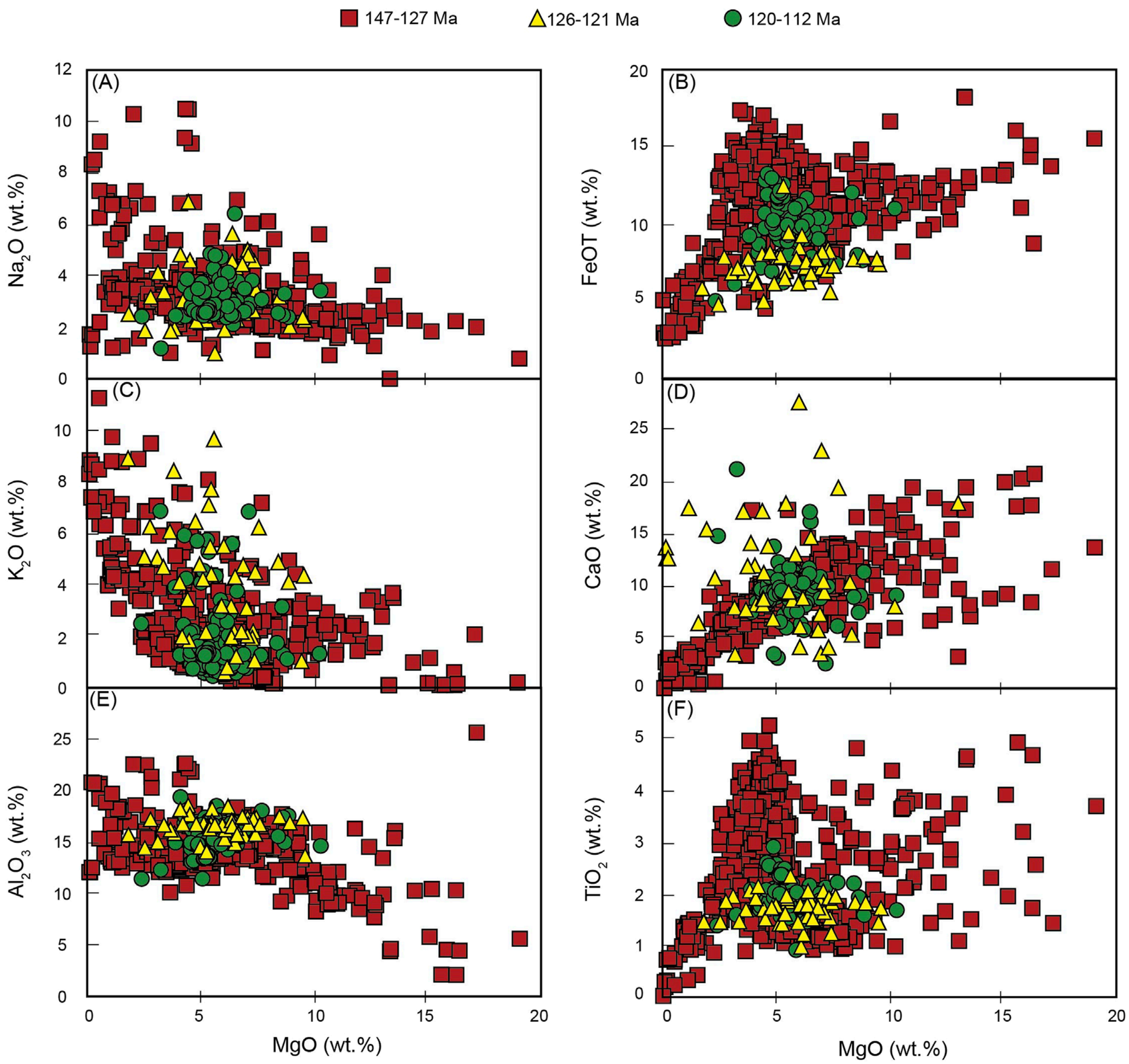

FIGURE 6
Variations in Na_2O **(A)**, FeOT **(B)**, K_2O **(C)**, CaO **(D)**, Al_2O_3 **(E)**, TiO_2 **(F)** vs MgO for igneous rocks from 147 Ma to 112 Ma. All data are provided in Supplementary Material.

settings. In this context, two key processes play a significant role: fractional crystallization and crustal contamination. Fractional crystallization appears to shape the geochemical characteristics of these rock at different levels. Whereas crustal contamination has likely influenced the geochemical signatures of rocks at different periods, as evidenced by the discrepancies of certain trace element ratios. Therefore, it is important to assess the influence of fractional crystallization and crustal contamination on the composition of these volcanic rocks.

In 147–127 Ma, the samples are mostly emplaced at the Paraná Basin and identified as continental flood basalts. The collected data indicate that the 147–127 Ma igneous rocks show strong correlations between MgO and other major oxides. As the MgO content decreases, the Na_2O, K_2O and Al_2O_3 contents increase, but the FeO, CaO, and TiO_2 decrease (Figure 6). The decrease of CaO and FeO is indicative of the early crystallization of Olivine and Pyroxene. Meanwhile, Na and K being incompatible elements, remain concentrated in the residuals, aligning with the negative correlations between Na_2O, K_2O, and MgO. Subsequently, the decline in TiO_2 suggests the crystallization of Ilmenite, corresponding to the decrease of FeO. In the later stage, the crystallization of Plagioclase crystallization became evident, as demonstrated by the negative correlation between Al_2O_3 and MgO. Before evaluating the presence of the crustal contamination, it needs to be pointed out that different elements are mobile during these processes (e.g., Sr, K), yet others remained relatively stable (e.g., Ti,

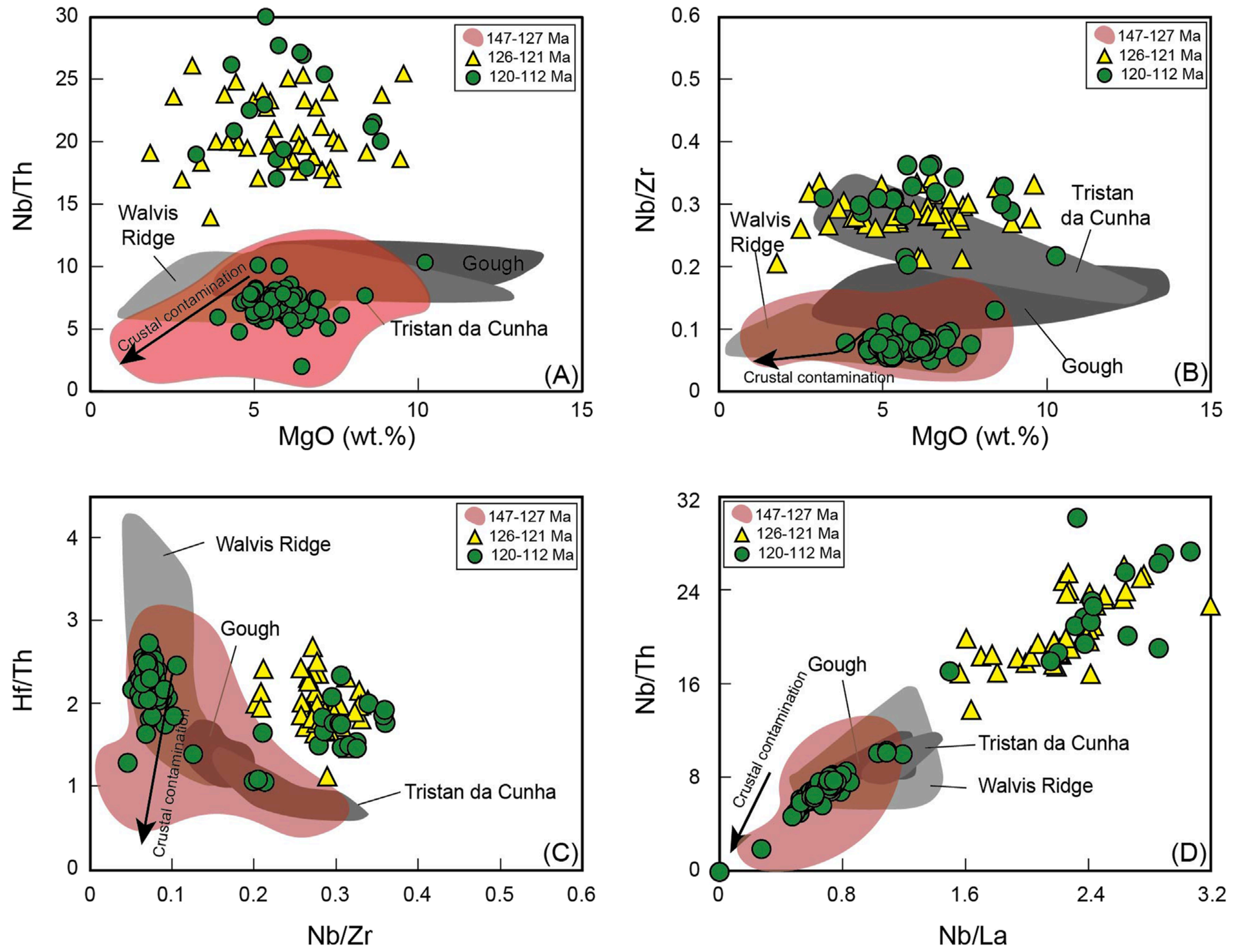

FIGURE 7
Major and trace element ratios relationship (Nb/Th vs MgO **(A)**, Nb/Zr vs MgO **(B)**, Hf/Th vs Nb/Zr **(C)**, Nb/Th vs Nb/La **(D)**) of igneous rocks from 147 Ma to 112 Ma. Modified from He et al. (2025). All data are provided in Supplementary Material. The crustal contamination line is from Marques et al. (2018). Lava flow are from the Walvis Ridges and the ocean islands of Tristan da Cunha and Gough Hoernle et al. (2015), Salters and Sachi-Kocher, (2010), Willbold and Stracke, (2006), Salters et al. (2011), Willbold and Stracke, (2010), and Weaver et al. (1987). The three locality are members of the Tristan mantle plume (Homrighausen et al., 2019; O'Connor and Jokat, 2015; Gibson et al., 2005).

Zr, Y, Nb, Th, and Nd) (Adriano et al., 2022; Bea, 2009; Kuritani et al., 2005; Smith and Smith, 1976). Thus, Nb, Th, Zr, Hf, La are selected here to verify the crustal contamination process as they are strongly incompatible LILEs and HFSEs which tend to remain in the melts other than minerals. Additionally, certain ratios such as Nb/Th, Nb/Zr, Hf/Th, Nb/La have generally distinct features (for the igneous rocks from mantle plume, Nb/Th: 5–15, Nb/Zr: 0–0.4, Hf/Th: 0.5–4.5, Nb/La: 0.4–1.5) and changes if contaminated by the crustal materials. The 147–127 Ma igneous rocks show clear signs of crustal contamination, evidenced by the progressive decrease in Nb/Th and Nb/Zr ratios co-occurring with the decline in MgO content, alongside the relatively low Hf/Th and Nb/La ratios (Figure 7). Within the lithosphere, Th exhibits significant enrichment over Nb and Hf, while Nb and Zr concentrations remain relatively stable in the mantle. Moreover, La preferentially remains in the melt phase rather than being incorporated into minerals, unlike Nb, which tends to be partitioned into specific mineral phases. Consequently, the incorporation of crustal materials causes decreases in Nb/Th and Nb/Zr ratios, and low Hf/Th and Nb/La ratios.

In 126–112 Ma, correlations between MgO and other major oxides are not found, indicating no fractional crystallization happened. The 126–121 Ma reveals no crustal material mixing as the absence of correlations between MgO, Nb/Th, Nb/Zr, and the high ratio of Hf/Th and Nb/La (He et al., 2025). Similarly, the absence of correlations between MgO and other major oxides of igneous rocks in 120–112 Ma indicates no fractional crystallization. Further analysis of trace elements can be taken into consideration. On the other hand, the igneous rocks at 120–112 Ma display more complicated characteristics; samples that overlap the mantle plume composition have crustal contamination signatures, while others proved none. The group overlaps with the mantle plume are also from the Paraná Basin dated to different periods and the reasons of crustal contamination are discussed above.

In 87–66 Ma, strong correlations are observed in the igneous rocks (Figure 8), where the Na_2O, K_2O, Al_2O_3 contents

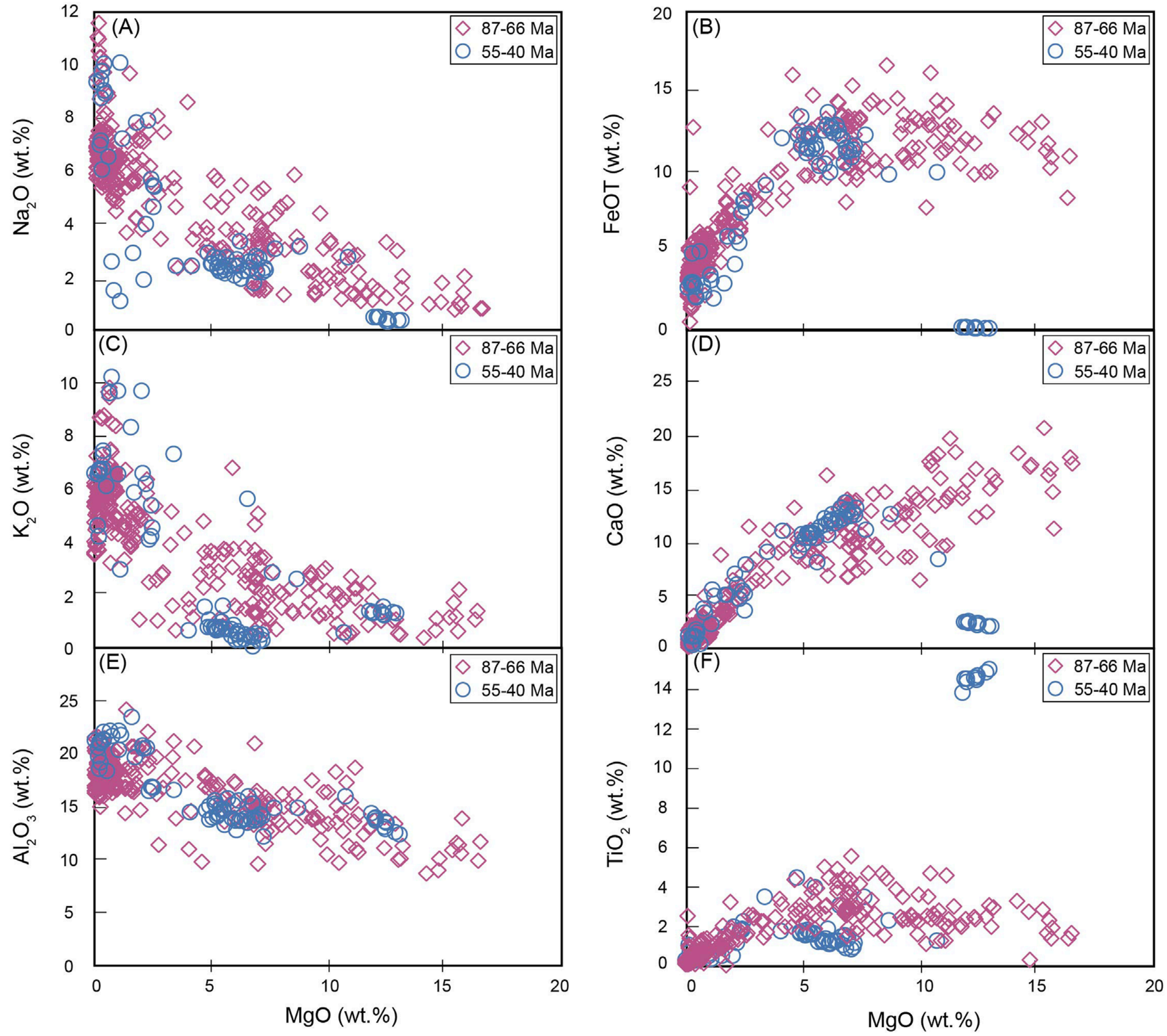

FIGURE 8
Variations in Na_2O **(A)**, FeOT **(B)**, K_2O **(C)**, CaO **(D)**, Al_2O_3 **(E)**, TiO_2 **(F)** vs MgO for igneous rocks from 87 Ma to 40 Ma. All data are provided in Supplementary Material.

increase, while FeO, CaO, TiO_2 decrease with decreasing MgO. The reduction in CaO and FeO signals the formation of olivine and pyroxene. Concurrently, Na_2O and K_2O, being incompatible elements, are concentrated in melts, which corresponds to the inverse relationships observed between them and MgO. Following this, the drop in TiO_2 indicates the crystallization of Ilmenite, which is associated with the decrease in FeO. In the final stage, the crystallization of Plagioclase becomes apparent, as evidenced by the negative correlation between Al_2O_3 and magnesium oxide MgO. Only a weak correlation between Hf/Th and Nb/Zr can be found, suggesting little or no crustal contamination.

In 55–40 Ma, strong linear correlations are shown between Al_2O_3, FeO, CaO, TiO_2, and MgO, unlike earlier rocks, the correlations between Na_2O, K_2O, and MgO are less obvious. The positive relations of FeO, CaO, and MgO indicate the crystallization of Olivine and Pyroxene. Also, the variation of FeO and TiO_2 shows the crystallization of Ilmenite. Lastly, the linear trend of Al_2O_3 reveals the crystallization of plagioclase. During this period, relatively strong crustal contamination is indicated by the decreasing trends between Nb/Th, Nb/Zr and MgO, Hf/Th and Nb/Zr of samples from this period reveal crustal contamination at a lower level (Figure 9). Different from earlier rocks, only no correlation displayed between Nb/Th and Nb/La. This could be attributed to different sources of crustal material where elements are enriched at various levels. Still, other correlations proved crustal contamination during this period.

At 147–127 Ma, 87–66 Ma, and 55–40 Ma, all or portions of the sample show evidence of fractional crystallization and varying degrees of crustal contamination, posing challenges to further analysis. On the other hand, for the igneous rocks at 126–121 Ma and 120–112 Ma, direct analysis of the source region is more feasible, as these rocks likely represent primary magma.

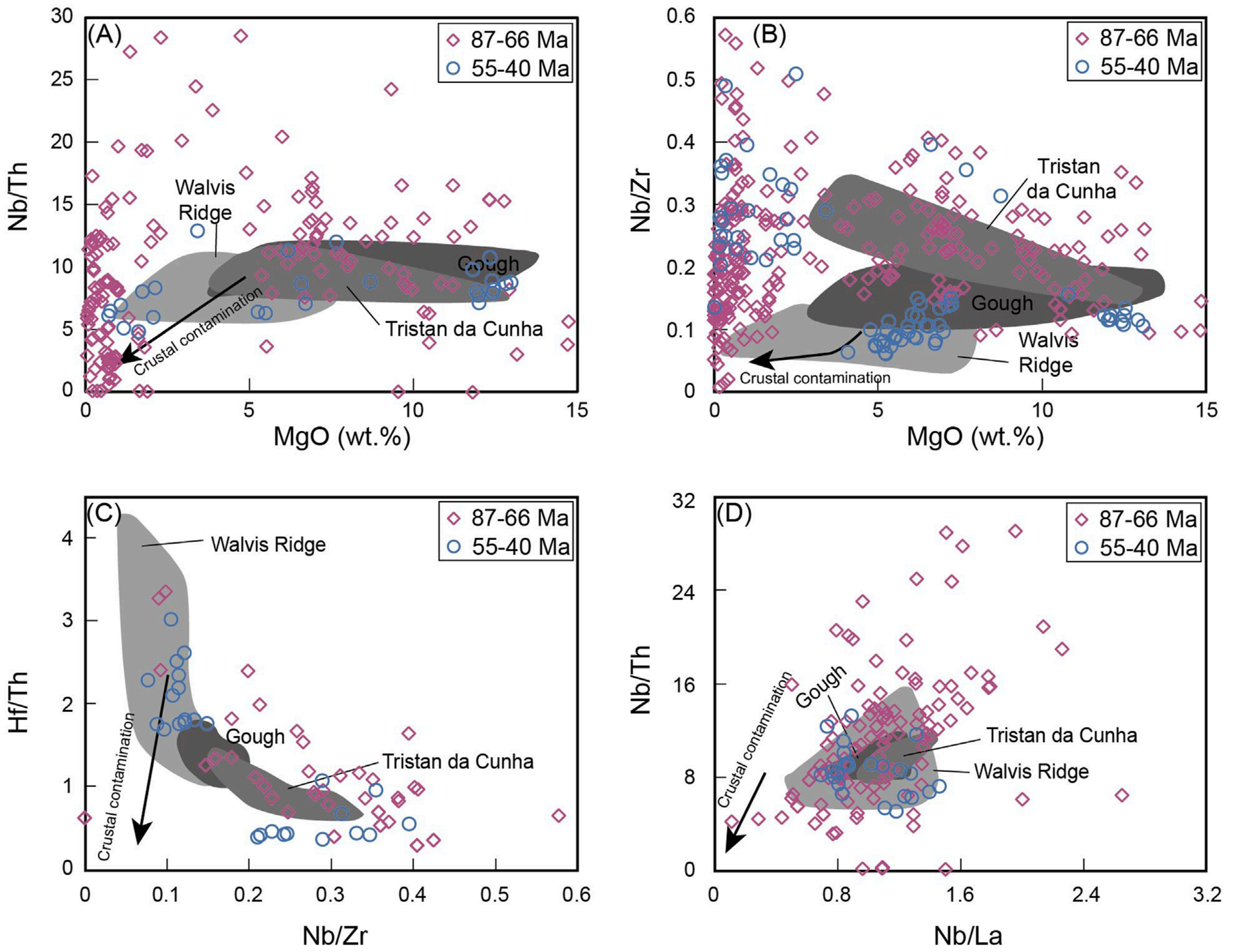

FIGURE 9
Major and trace element ratios relationship (Nb/Th vs MgO **(A)**, Nb/Zr vs MgO **(B)**, Hf/Th vs Nb/Zr **(C)**, Nb/Th vs Nb/La **(D)**) of igneous rocks from 87 Ma to 40 Ma. Modified from He et al. (2025). All data are provided in Supplementary Material. The crustal contamination line is from Marques et al. (2018). Lava flow are from the Walvis Ridges and the ocean islands of Tristan da Cunha and Gough are from Hoernle et al. (2015), Salters and Sachi-Kocher, (2010), Willbold and Stracke, (2006), Salters et al. (2011), Willbold and Stracke, (2010), and Weaver et al. (1987). The three locality are members of the Tristan mantle plume (Homrighausen et al., 2019; O'Connor and Jokat, 2015; Gibson et al., 2005).

5.2 Influence of the mantle plume and continental rift

Igneous rocks emplaced at different periods from Santos basin and adjacent areas show variable geochemical and isotopic compositions, indicating different source regions and evolutionary paths.

Basalts emplaced during 147–127 Ma are coeval with the Tristan mantle plume at ~135–132 Ma (Hoernle et al., 2015; Rohde et al., 2013; Renne et al., 2011; Renne et al., 1996; Segev, 2002) in Paraná Basin. The geochemical characteristics of igneous rocks during this period are similar to magmas with mantle plume origin. Firstly, the low Nb/Zr, Nb/Th and Nb/La ratios of igneous rocks display similarity to the rocks generated by the Tristan mantle plume system (Figure 7). Moreover, the wide range of initial $^{87}Sr/^{86}Sr$ and negative $\varepsilon Nd_{(t)}$ (Figure 5) point to potential similarity to the Tristan mantle plume characteristics as discussed in previous studies (Zhou et al., 2022; Homrighausen et al., 2019). Seismic evidences (P-wave finite-frequence traveltime, Rayleigh-wave phase velocity and receiver function) and geophysical modeling also confirm the existence of the Tristan mantle plume system and its influence (Geissler et al., 2020; Bonadio et al., 2018; Yuan et al., 2017; Schlömer, 2016). As the mantle plume ascends, it inevitably interacts with and incorporates lithospheric mantle and crustal materials, resulting in geochemical and isotopic signatures indicative of fractional crystallization and crustal contamination. Such a process is consistent with the observed geochemical features of this period, provides a reasonable explanation for their evolution, and discloses their mantle plume origin.

The trace elements of basalts and diabases emplaced at 126–112 Ma show high Nb/Th, Nb/Zr, Nb/La, whose trace elements characteristics plot all away from the mantle plume composition, excluding their mantle plume origin (Figure 7). Enriched Sr and Nd isotopic compositions show similar characteristics to Continental Rift basalts instead of Ocean Island Basalts (OIB) (Figure 10), and can be divided into two groups based on their ages, 126–121 Ma and 120–112 Ma. The REE fraction modeling

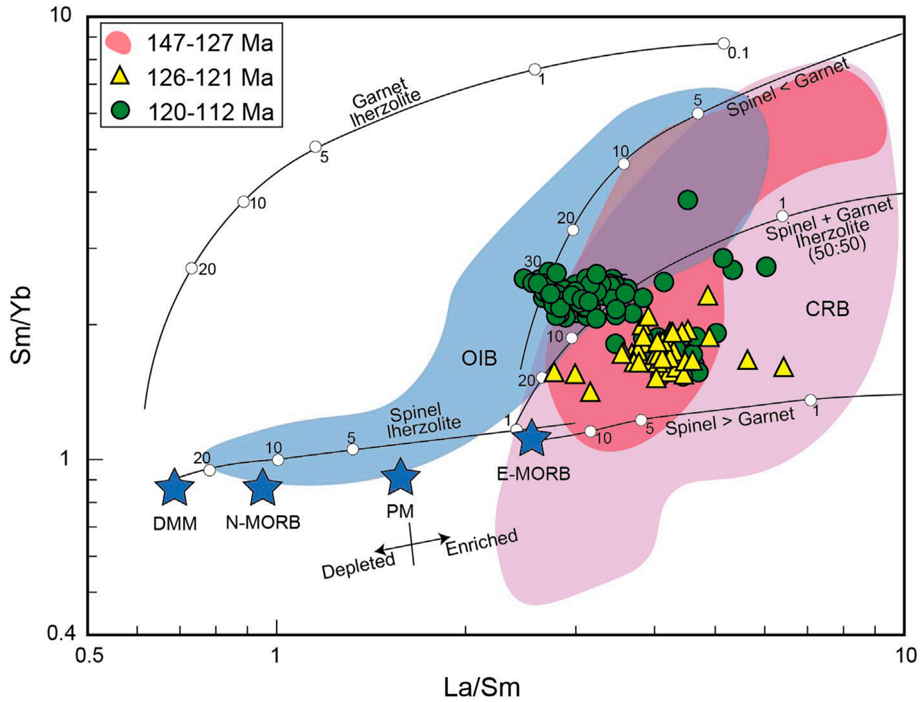

FIGURE 10
Variations in La/Sm vs Sm/Yb for igneous rocks from 147 Ma to 112 Ma. Modified from He et al. (2025). All data are provided in Supplementary Material. The field of global continental rift basalt (CRB) and Ocean Island basalts (OIB) are from the PetDB database (https://search.earthchem.org/). DMM, depleted mid-ocean ridge basalt mantle; PM, primitive mantle, N-MORB, normal mid-ocean ridge basalt, E-MORB, enriched mid-ocean ridge basalt. The white-doted numbers stand for different partial melting degrees.

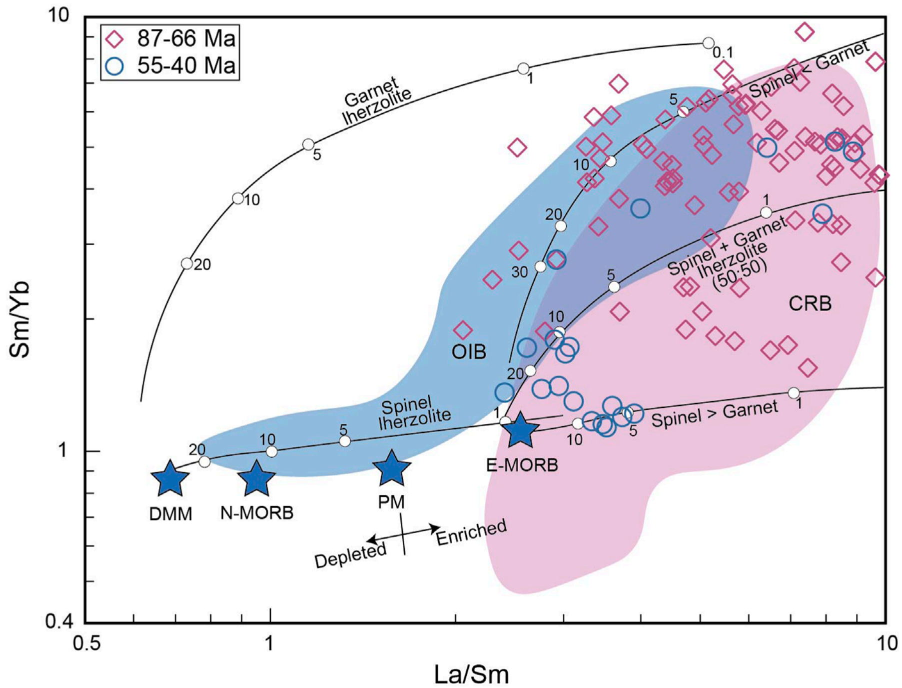

FIGURE 11
Variations in La/Sm vs Sm/Yb for igneous rocks from 87 Ma to 40 Ma. Modified from He et al. (2025). All data are provided in Supplementary Material. The field of global continental rift basalt (CRB) and Ocean Island basalts (OIB) are from the PetDB database (https://search.earthchem.org/). DMM, depleted mid-ocean ridge basalt mantle; PM, primitive mantle, N-MORB, normal mid-ocean ridge basalt, E-MORB, enriched mid-ocean ridge basalt. The white-doted numbers stand for different partial melting degrees.

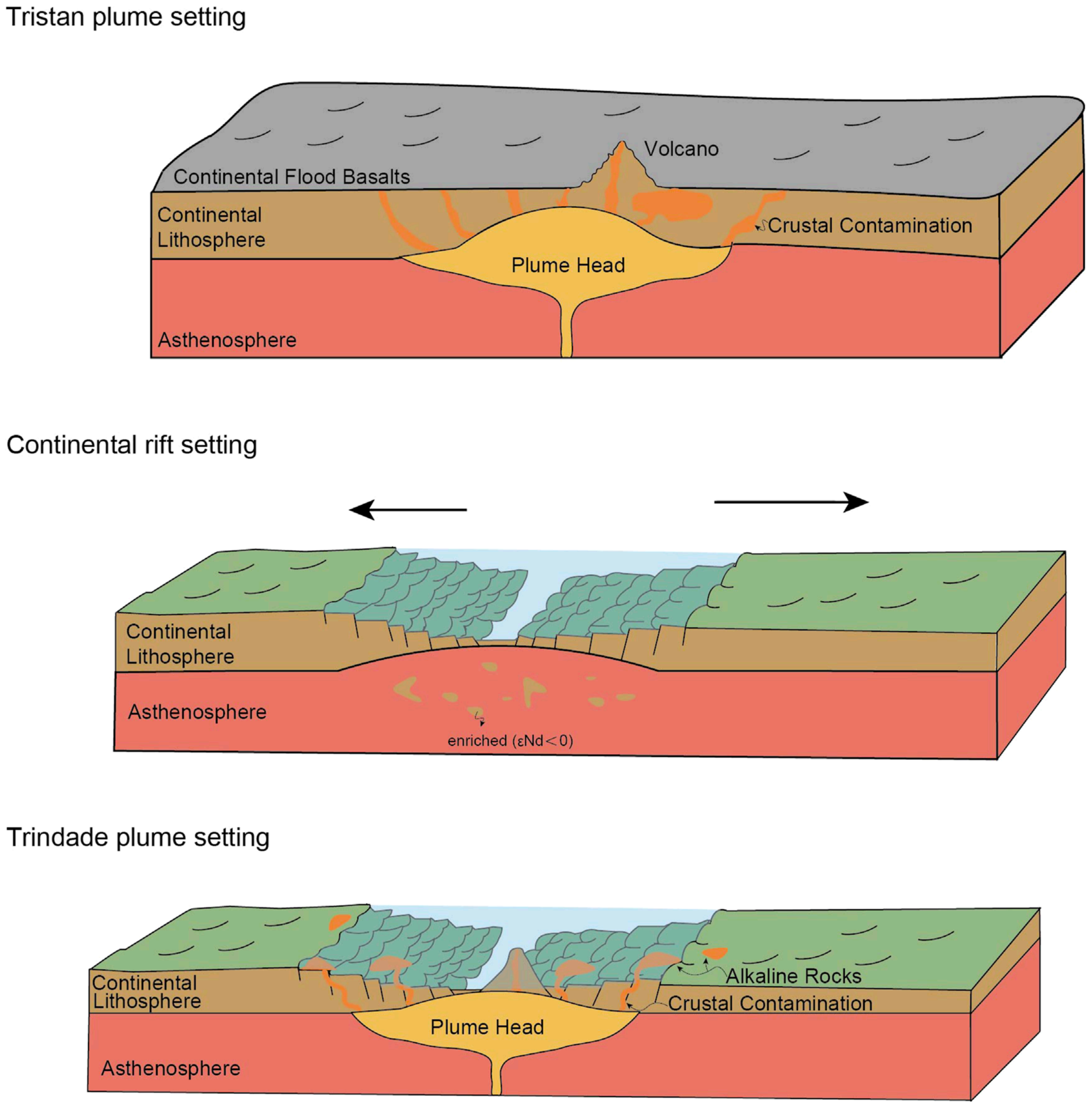

FIGURE 12
The modal diagrams of the proposed tectonic evolution of the studied area, modified from He et al. (2025).

suggests basalts at 126–121 Ma originated from the Spinel + Garnet (Spinel/Garnet>1) lherzolite face with 1%–5% partial melting. The high La/Sm ratios of the rocks display similarity to the rift basalts other than OIB. Whereas basaltic rocks at 120–112 Ma, modeling results show a deeper source region, from Spine + Garnet (Spinel/Garnet<1) lherzolite face with evidently higher partial melting degree (5%–10%), the rather low Sm/Yb ratios still point to similarity to the rift basalts. Lastly, the isotopic composition discloses the source region from the depleted mantle to the slightly enriched mantle, which is explained as the involvement of crustal materials during 120–112 Ma (He et al., 2025). Therefore, the origin of mafic rocks during 126–112 Ma are generated from the continental rift, and the rift extended from shallow to deeper asthenosphere (He et al., 2025).

Igneous rocks emplaced at 87–40 Ma show completely different geochemical characteristics from rocks emplaced during 127–112 Ma. Although modeling result shows samples have higher La/Sm and Sm/Yb ratios, and plot into Spinel + Garnet lherzolite facies (Figure 11), which is similar to the continental rift basalts, it contradicts the area history that rift activity ends at ~113 Ma (Moreira et al., 2007; Mohriak and Rosendahl, 2003). The relative low ratios of Nb/Th, Nb/La, and the wide range of Nb/Zr prove a connection between their source and the mantle plume (Figure 9). Moreover, the initial Nd values resemble the OIB (Figure 5). Previous geochemical and geochronological evidence also confirm existence of the mantle plume at this period (Santos et al., 2021; Gibson et al., 2005; Gibson et al., 1995). Hence, from 87 to 40 Ma, the igneous rocks are derived from mantle plume.

Combining the major, trace element and isotopic compositions, the tectonic context of each episode can be revealed. In 147–127 Ma, the igneous rocks are from mantle plume source, carrying characteristics from the lithosphere inevitably incorporated during ascending. Then, magmatism occurred within a continental rift setting from 126 to 112 Ma. Lastly, during 87–40 Ma, the igneous rocks are under the influence of mantle plume. It is important to note that these tectonic activities have the potential to facilitate hydrocarbon generation. The mantle plume and continental rifting significantly influenced hydrocarbon generation in the Santos Basin by introducing heat that matured organic-rich source rocks like the Itapema Formation shales. Magmatic activity, including Aptian and Santonian-Campanian phases, created igneous complexes and local paleohighs, which acted as reservoirs or traps for hydrocarbons. The combined effects of the plume and rifting enhanced the basin's hydrocarbon potential (Yan et al., 2024; Ismail-Zadeh et al., 2024; Zhao et al., 2023; Brune et al., 2023).

5.3 Geodynamic

Southeast Brazil's passive continental margin and adjacent areas suffered a complex tectonic background from 147 to 40 Ma, including mantle plume, rifting, extension, and drift (He et al., 2025; Pinheiro and Cianfarra, 2021; Cogné et al., 2012; Assumpção et al., 2004; Assumpção., 1998). The Tristan da Cunha mantle plume began to uplift since ~135 Ma, a process that is associated with the breakup of Gondwana and the subsequent opening of the South Atlantic Ocean during the Lower Cretaceous period (Chang et al., 1992; Cainelli and Mohriak, 1999). Around 85 Ma, the Trindade mantle plume became active, generating a series of alkaline rocks, with its influence persisting into the Eocene (Maia et al., 2021; Rocha et al., 2011; Thompson et al., 1998; Gibson et al., 1995).

The Tristan da Cunha mantle plume rose and formed huge amounts of flood basalts with crustal signatures. The thermal effects brought by the mantle plume heated and softened the overlying strata, leading to significant uplifting. From 126 to 112 Ma, the mantle plume's contribution only exists in heat conduction. The magmas are sourced from Spinel + Garnet (Spinel/Garnet>1) lherzolite face and then shifted to Spine + Garnet (Spinel/Garnet<1) lherzolite face, which is from shallow asthenosphere to deeper asthenosphere. In the meantime, the partial melting degree of this period's igneous rocks increased from 1%–5% to 5%–10%. At this stage, the geochemical characteristics correspond to the onset of rift activity, where the mantle plume-induced heating, combined with thinning and stretching of the lithosphere, deepened the source region. Such a process facilitated the mixing of crustal material, and altered the pressure, thereby allowing for a higher degree of partial melting. After the disclosure of rift activity, the igneous rocks are then sourced from the ascending mantle plume, with crustal material signature caused by up-welling (Figure 12).

6 Conclusion

This study compiled the geochemical data of the Santos Basin and adjacent areas, whose age ranges from 147 Ma to 40 Ma. The geochemical features and their tectonic implications bring new insight into the magmatic movements on the passive margin. The source composition varies from the mantle plume to different depths of the asthenosphere, with mixing of crustal material at certain periods. The geological model indicates that the mantle plume initiated the rift and heated the overlying lithosphere, resulting in continental thinning and stretching. The research provides more perspectives in understanding the correlations between magmatism and basin dynamics.

Author contributions

JS: (1st author): Writing–original draft, Writing–review and editing, Data curation. JS (2nd author): Writing–original draft, Writing–review and editing, Data curation. LY: Data curation, Writing–review and editing.

Funding

The author(s) declare that no financial support was received for the research, authorship, and/or publication of this article.

Conflict of interest

The authors declare that the research was conducted in the absence of any commercial or financial relationships that could be construed as a potential conflict of interest.

Generative AI statement

The author(s) declare that no Generative AI was used in the creation of this manuscript.

Publisher's note

Supplementary material

The Supplementary Material for this article can be found online at: https://www.frontiersin.org/articles/10.3389/feart.2025.1560988/full#supplementary-material

References

Adriano, M. S., Figueiredo, J. P., Coelho, P. H. G. R., and Borghi, L. (2022). Tectonic and stratigraphic evolution of the Santos Basin rift phase: new insights from seismic interpretation on Tupi oil field area. *J. S. Am. Earth Sci.* 116, 103842. doi:10.1016/j.jsames.2022.103842

Anjos, S., Sombra, C., and Spadini, A. (2024). The evolution of oil and gas exploration and development in Brazil: from onshore to ultra-deepwater. *Petroleum Explor. and Dev.* 51, 796–806. Available at: https://link.cnki.net/urlid/11.2360.TE.20240724.2308.004.

Assumpção, M. (1998). Seismicity and stresses in the Brazilian passive margin. *Bull. Seismol. Soc. Am.* 88, 160–169. doi:10.1785/BSSA0880010160

Assumpçao, M., Schimmel, M., Escalante, C., Roberto Barbosa, J., Rocha, M., and Barros, L. V. (2004). Intraplate seismicity in SE Brazil: stress concentration in lithospheric thin spots. *Geophys. J. Int.* 159, 390–399. doi:10.1111/j.1365-246X.2004.02357.x

Bas, M. L., Maitre, R. L., Streckeisen, A., Zanettin, B., and Rocks, I. S. O. T. S. O. I. (1986). A chemical classification of volcanic rocks based on the total alkali-silica diagram. *J. Petrology* 27, 745–750. doi:10.1093/petrology/27.3.745

Bea, F. (2009). Behavior of trace elements during magma genesis and evolution. *GEOLOGY* II, 186.

Bonadio, R., Geissler, W. H., Lebedev, S., Fullea, J., Ravenna, M., Celli, N. L., et al. (2018). Hot upper mantle beneath the Tristan da Cunha hotspot from probabilistic Rayleigh-wave inversion and petrological modeling. *Geochem. Geophys. Geosystems* 19, 1412–1428. doi:10.1002/2017GC007347

Brune, S., Kolawole, F., Olive, J. D., Sarah Stamps, D., Roger Buck, W., Buiter, B., et al. (2023). Geodynamics of continental rift initiation and evolution. *Nat. Rev. Earth and Environ.* 4, 235–253. doi:10.1038/s43017-023-00391-3

Buckley, J., Bosence, D., and Elders, C. (2015). Tectonic setting and stratigraphic architecture of an early cretaceous lacustrine carbonate platform, sugar loaf high, Santos Basin, Brazil. *Geological Society, London, Special Publications* 418, 175–191. doi:10.1144/SP418.13

Cainelli, C., and Mohriak, W. U. (1999). General evolution of the eastern Brazilian continental margin. *Lead. Edge* 18, 800–805. doi:10.1190/1.1438387

Chang, H. K., Kowsmann, R. O., Figueiredo, A. M. F., and Bender, A. (1992). Tectonics and stratigraphy of the East Brazil Rift system: an overview. *Tectonophysics* 213, 97–138. doi:10.1016/0040-1951(92)90253-3

Chen, C., Gao, Y., Zhang, X., Zhao, R., Pan, Y., Li, C., et al. (2018). Characteristics of sedimentary layers in volcanic stratigraphy and their stratigraphic comparative significance: an example from the Yingcheng Formation in the Songliao Basin. *J. Earth Sci.* 43 (03), 812–826.

Cheng, T., Kang, H., Liang, J., Jia, H., Bai, B., and Li, M. (2019). Classification of magmatic rock genesis and analysis of activity periods in the Santos Basin, Brazil. *China Offshore Oil Gas* 31 (04), 55–66.

Cogné, N., Gallagher, K., Cobbold, P. R., Riccomini, C., and Gautheron, C. (2012). Post-breakup tectonics in southeast Brazil from thermochronological data and combined inverse-forward thermal history modeling. *J. Geophys. Res. Solid Earth* 117. doi:10.1029/2012JB009340

Dos Santos, A. C., Mata, J., Jourdan, F., De Oliveira Rodrigues, S. W., Monteiro, L. G. P., Guedes, E., et al. (2021). Martin Vaz island geochronology: constraint on the Trindade Mantle Plume track from the youngest and easternmost volcanic episodes. *J. S. Am. Earth Sci.* 106, 103090. doi:10.1016/j.jsames.2020.103090

Eagles, G. (2007). New angles on South Atlantic opening. *Geophys. J. Int.* 168, 353–361. doi:10.1111/j.1365-246X.2006.03206.x

Eagles, G., and Eisermann, H. (2020). The Skytrain plate and tectonic evolution of southwest Gondwana since Jurassic times. *Sci. Rep.* 10, 19994. doi:10.1038/s41598-020-77070-6

Feng, M., An, M., Zang, H., Assumpção, M. S., Bianchi, M. B., França, G. S., et al. (2024). Dynamic evolution of West Gondwana inferred from crustal anisotropy of the South American platform. *Geophys. J. Int.* 239, 201–217. doi:10.1093/gji/ggae267

Gao, D. (2022). Continental tapering of South America caused asymmetric non-uniform opening of the South Atlantic Ocean. *Commun. Earth and Environ.* 3, 278. doi:10.1038/s43247-022-00587-3

Geissler, W. H., Wintersteller, P., Maia, M., Strack, T., Kammann, J., Eagles, G., et al. (2020). Seafloor evidence for pre-shield volcanism above the Tristan da Cunha mantle plume. *Nat. Commun.* 11, 4543. doi:10.1038/s41467-020-18361-4

Gibson, S., Thompson, R., Day, J., Humphris, S., and Dickin, A. (2005). Melt-generation processes associated with the Tristan mantle plume: constraints on the origin of EM-1. *Earth Planet. Sci. Lett.* 237, 744–767. doi:10.1016/j.epsl.2005.06.015

Gibson, S., Thompson, R., Leonardos, O., Dickin, A., and Mitchell, J. (1995). The Late Cretaceous impact of the Trindade mantle plume: evidence from large-volume, mafic, potassic magmatism in SE Brazil. *J. Petrology* 36, 189–229. doi:10.1093/petrology/36.1.189

Gordon, A. C., Santos, A. C., Caitano, G. R., Stanton, N., and Mohriak, W. U. (2023). Magmatic cycles in Santos Basin (S.E. Brazil): geochemical characterization and magmatic sources. *J. S. Am. Earth Sci.* 126, 104323. doi:10.1016/j.jsames.2023.104323

Guo, B., Geng, W., Chen, H., Li, P., Jia, N., and Wang, L. (2022). Reservoir prediction of Permian igneous rocks in Chengdu-Jianyang area. *Oil Geophys. Prospect.* 57, 104–109+11. Available at: https://link.cnki.net/doi/10.13810/j.cnki.issn.1000-7210.2022.S1.016.

He, W., Wang, H., Su, J., Wang, W., Zhao, J., Zuo, G., et al. (2025). Magma evolution during the post-rift phase of the Santos Basin, Brazil: petrogenesis and geochemistry of ~126–121 ma basalts and diabases. *Front. Earth Sci.* 12, 1497913. doi:10.3389/feart.2024.1497913

Hoernle, K., Rohde, J., Hauff, F., Garbe-Schönberg, D., Homrighausen, S., Werner, R., et al. (2015). How and when plume zonation appeared during the 132 Myr evolution of the Tristan Hotspot. *Nat. Commun.* 6, 7799–7810. doi:10.1038/ncomms8799

Homrighausen, S., Hoernle, K., Hauff, F., Wartho, J.-A., Van Den Bogaard, P., and Garbe-Schönberg, D. (2019). New age and geochemical data from the Walvis Ridge: the temporal and spatial diversity of South Atlantic intraplate volcanism and its possible origin. *Geochimica Cosmochimica Acta* 245, 16–34. doi:10.1016/j.gca.2018.09.002

Ismail-Zadeh, A., Davaille, A., Besse, J., and Volozh, Y. (2024). East European sedimentary basins long heated by a fading mantle upwelling. *Nat. Commun.* 15, 3915. doi:10.1038/s41467-024-48127-1

Jiang, H., Ju, B., Jiang, L., Qi, R., and Li, L. (2011). Current situation and prospect of world igneous oil and gas exploration and development. *Special Oil and Gas Reservoirs* 18 (02), 1–6+135.

Jin, Q., Wan, C., and Zhou, F. (2006). Migration of trace elements from Minqiao basalt in the Jinhu Depression to hydrocarbon source rocks and its geological significance. *J. China Univ. Petroleum*, 1–5.

Jin, Q., and Zhai, Q. (2003). Volcanic hydrothermal activity and hydrocarbon generation in the Rift Basin. *Chin. J. Geol.*, 342–934.

Kuritani, T., Kitagawa, H., and Nakamura, E. (2005). Assimilation and fractional crystallization controlled by transport process of crustal melt: implications from an alkali basalt–dacite suite from rishiri volcano, Japan. *J. Petrology* 46, 1421–1442. doi:10.1093/petrology/egi021

Liu, R., and Liu, Z. (2006). Current status and comprehensive development potential analysis of oil shale resources at home and abroad. *J. Jilin Univ.*, 892–898. Available at: https://link.cnki.net/doi/10.13278/j.cnki.jjuese.2006.06.004.

Liu, Y., Wang, D., Tian, Z., Zhang, Z., Wang, T., Wang, C., et al. (2023). Characterization and prediction of igneous rock development in complex carbonate fields in the Santos Basin, Brazil. *Lithol. Reserv.* 35 (06), 127–137. Available at: https://link.cnki.net/urlid/62.1195.TE.20230809.1357.

Luo, B., Xia, M., Wang, H., Fan, Y., Xu, L., Liu, R., et al. (2019). Analysis of gas reservoir formation conditions in permian volcanic rocks in the western Sichuan Basin. *Nat. Gas. Ind.* 39 (02), 9–16. Available at: https://link.cnki.net/urlid/51.1179.TE.20190225.2116.004.

Maia, T. M., Dos Santos, A. C., Rocha-Júnior, E. R. V., De Morisson Valeriano, C., Mendes, J. C., Jeck, I. K., et al. (2021). First petrologic data for Vitória seamount, Vitória-Trindade Ridge, South Atlantic: a contribution to the trindade mantle plume evolution. *J. S. Am. Earth Sci.* 109, 103304. doi:10.1016/j.jsames.2021.103304

Marques, L., De Min, A., Rocha-Júnior, E., Babinski, M., Bellieni, G., and Figueiredo, A. (2018). Elemental and Sr-Nd-Pb isotope geochemistry of the Florianópolis Dyke Swarm (Paraná Magmatic Province): crustal contamination and mantle source constraints. *J. Volcanol. Geotherm. Res.* 355, 149–164. doi:10.1016/j.jvolgeores.2017.07.005

Mohriak, W., and Rosendahl, B. (2003). Transform zones in the South Atlantic rifted continental margins. *Geol. Soc. Lond. Spec. Publ.* 210, 211–228. doi:10.1144/GSL.SP.2003.210.01.13

Mohriak, W. U., Szatmari, P., and Anjos, S. (2012). Salt: geology and tectonics of selected Brazilian basins in their global context. *Geol. Soc. Lond. Spec. Publ.* 363, 131–158. doi:10.1144/SP363.7

Moreira, J. L. P., Madeira, C. V., Gil, J. A., and Machado, M. a. P. (2007). bacia de Santos. *Bol. Geociencias PETROBRAS* 15, 531–549.

Mu, L., and Ji, Z. (2019). Progress and development direction of PetroChina's overseas oil and gas exploration theory and technology. *Petroleum Explor. Dev.* 46 (06), 1027–1036. Available at: https://link.cnki.net/urlid/11.2360.TE.20191008.1111.004.

O'Connor, J. M., and Jokat, W. (2015). Age distribution of Ocean Drill sites across the Central Walvis Ridge indicates plate boundary control of plume volcanism in the South Atlantic. *Earth Planet. Sci. Lett.* 424, 179–190.

Pinheiro, M. R., and Cianfarra, P. (2021). Brittle deformation in the Neoproterozoic basement of southeast Brazil: traces of intraplate Cenozoic tectonics. *Geosciences* 11, 270. doi:10.3390/geosciences11070270

Renne, P. R., Balco, G., Ludwig, K. R., Mundil, R., and Min, K. (2011). Response to the comment by WH Schwarz et al. on "Joint determination of ^{40}K decay constants and ^{40}Ar/^{40}K for the Fish Canyon sanidine standard, and improved accuracy for ^{40}Ar/^{39}Ar geochronology". *Geochimica Cosmochimica Acta* 75, 5097–5100. doi:10.1016/j.gca.2011.06.021

Renne, P. R., Glen, J. M., Milner, S. C., and Duncan, A. R. (1996). Age of Etendeka flood volcanism and associated intrusions in southwestern Africa. *Geology* 24, 659–662. doi:10.1130/0091-7613(1996)024<0659:AOEFVA>2.3.CO;2

Rocha, M. P., Schimmel, M., and Assumpçao, M. (2011). Upper-mantle seismic structure beneath SE and Central Brazil from P-and S-wave regional traveltime tomography. *Geophys. J. Int.* 184, 268–286. doi:10.1111/j.1365-246X.2010.04831.x

Rohde, J. K., van den Bogaard, P., Hoernle, K., Hauff, F., and Werner, R. (2013). Evidence for an age progression along the Tristan-Gough volcanic track from new ^{40}Ar/^{39}Ar ages on phenocryst phases. *Tectonophysics* 604, 60–71.

Salters, V. J., Mallick, S., Hart, S. R., Langmuir, C. E., and Stracke, A. (2011). Domains of depleted mantle: new evidence from hafnium and neodymium isotopes. *Geochem. Geophys. Geosystems* 12. doi:10.1029/2011GC003617

Salters, V. J., and Sachi-Kocher, A. (2010). An ancient metasomatic source for the Walvis Ridge basalts. *Chem. Geol.* 273, 151–167. doi:10.1016/j.chemgeo.2010.02.010

Schlömer, A. (2016). *Tristan da Cunha hotspot: Mantle plume or shallow plate tectonics? Doctoral dissertation*. Bremen, Germany: Universität Bremen.

Segev, A. (2002). Flood basalts, continental breakup and the dispersal of Gondwana: evidence for periodic migration of upwelling mantle flows (plumes). *EGU Stephan Mueller Special Publication Series* 2, 171–191. doi:10.5194/smsps-2-171-2002

Smith, R. E., and Smith, S. E. (1976). Comments on the use of Ti, Zr, Y, Sr, K, P and Nb in classification of basaltic magmas. *Earth Planet. Sci. Lett.* 32, 114–120. doi:10.1016/0012-821X(76)90049-2

Song, Z. (2009). *Study on the mechanism of hydrocarbon generation from igneous rocks to hydrocarbon source rocks in Yangxin depression*.

Suárez, R., Ghiglione, M. C., Sue, C., Quezada, P., Roy, S., Rojo, D., et al. (2021). Paleozoic-early Mesozoic structural evolution of the West Gondwana accretionary margin in southern Patagonia, Argentina. *J. S. Am. Earth Sci.* 106, 103062. doi:10.1016/j.jsames.2020.103062

Sun, S. S., and Mcdonough, W. F. (1989). Chemical and isotopic systematics of oceanic basalts: implications for mantle composition and processes. *Geol. Soc. Lond. Spec. Publ.* 42, 313–345. doi:10.1144/GSL.SP.1989.042.01.19

Thompson, R., Gibson, S., Mitchell, J., Dickin, A., Leonardos, O., Brod, J., et al. (1998). Migrating Cretaceous–Eocene magmatism in the Serra do Mar alkaline province, SE Brazil: melts from the deflected Trindade mantle plume? *J. Petrology* 39, 1493–1526. doi:10.1093/petroj/39.8.1493

Torsvik, T. H., Rousse, S., Labails, C., and Smethurst, M. A. (2009). A new scheme for the opening of the South Atlantic Ocean and the dissection of an Aptian salt basin. *Geophys. J. Int.* 177, 1315–1333. doi:10.1111/j.1365-246X.2009.04137.x

Wan, C., Jin, Q., and Zhai, Q. (2003). Role of submarine volcanic eruption on hydrocarbon source rock formation and hydrocarbon evolution in the Binnan area of the Dongying Depression. *J. China Univ. Petroleum Ed. Nat. Sci.* 03, 17–21+8.

Wang, C., Wang, H., Shao, D., Zhang, Y., and Li, D. (2018). Seismic prediction of igneous rocks in the S field, Santos Basin, Brazil. *Comput. Tech. Geophys. Geochem. Explor.* 40 (05), 573–578.

Wang, L., Li, H., Shi, Y., Zhao, Y., and Ma, Y. (2015). History and prospects of global volcanic reservoir research. *Geol. China* 42 (05), 1610–1620.

Weaver, B. L., Wood, D. A., Tarney, J., and Joron, J. L. (1987). Geochemistry of ocean island basalts from the south Atlantic: Ascension, Bouvet, St. Helena, Gough and Tristan da Cunha. *Geological Society, London, Special Publications* 30, 253–267. doi:10.1144/GSL.SP.1987.030.01.11

Willbold, M., and Stracke, A. (2006). Trace element composition of mantle end-members: implications for recycling of oceanic and upper and lower continental crust. *Geochem. Geophys. Geosystems* 7. doi:10.1029/2005GC001005

Willbold, M., and Stracke, A. (2010). Formation of enriched mantle components by recycling of upper and lower continental crust. *Chem. Geol.* 276, 188–197. doi:10.1016/j.chemgeo.2010.06.005

Winchester, J. A., and Floyd, P. A. (1977). Geochemical discrimination of different magma series and their differentiation products using immobile elements. *Chem. Geol.* 20, 325–343. doi:10.1016/0009-2541(77)90057-2

Yan, K., Zuo, Y., Zhang, Y., Yang, L., Peng, X., Wang, S., et al. (2024). A study on the accumulation model of the Santos basin in Brazil utilizing the source–reservoir dynamic evaluation method. *Sci. Rep.* 14, 19296. doi:10.1038/s41598-024-69756-y

Yu, T., Liu, Z., Wang, J., Meng, Q., and Li, Y. (2022). Geochemical characteristics and geological significance of the lower permian irati formation oil shale in the Paraná Basin, Brazil. *Coal Geol. China* 34 (08), 1–8.

Yuan, X., Heit, B., Brune, S., Steinberger, B., Geissler, W. H., Jokat, W., et al. (2017). Seismic structure of the lithosphere beneath NW Namibia: Impact of the Tristan da Cunha mantle plume. *Geochem. Geophys. Geosystems* 18, 125–141. doi:10.1002/2016gc006645

Zhai, Q., Jin, Q., Zeng, Y., and Wan, C. (2004). Hydrocarbon geologic characteristics of basalt-hydrocarbon source rock symbiosis in Binnan area, Dongying Depression, Bohai Bay Basin. *Petroleum Geol. and Exp.* 05, 448–451.

Zhang, Z., Zhu, Y., Zhang, D., Su, Y., Yao, W., Bao, Z., et al. (2020). The accumulation patterns and exploration insights of oil and gas in the subsalt carbonate reservoirs of the Campos Basin, Brazil. *China Pet. Explor.* 25 (04), 75–85.

Zhao, J., Zhao, J., Ren, K., Wang, H., Wang, C., Yang, X., et al. (2023). Multiple pulses eruption of Aptian magma and their key role in the deposition of coquinas limestone in the Itapema Formationin Block L, Santos basin. *Acta Geol. Sin.* 97, 539–552.

Zhou, H., Hoernle, K., Geldmacher, J., Hauff, F., Garbe-Schönberg, D., Jung, S., et al. (2022). Enriched mantle one (EMI) type carbonatitic volcanism in Namibia: evidence for a concentrically-zoned Etendeka plume head. *Gondwana Res.* 109, 239–252. doi:10.1016/j.gr.2022.04.014